Coating Process for MEMS Based 3-axis Force Sensors

Andres Ospina and Saifeddine Aloui
Laboratory of sensor system characterization
Commissariat à l'énergie atomique
et aux énergies alternatives
Grenoble, France
Email: andres.ospina@cea.fr and
saifeddine.aloui@cea.fr

Mathieu Grossard
Interactive Robotic Laboratory
Commissariat à l'énergie atomique
et aux énergies alternatives
Saclay, France
Email: mathieu.grossard@cea.fr

Alain Micaelli
Interactive Simulation Laboratory
Commissariat à l'énergie atomique
et aux énergies alternatives
Saclay, France
Email: alain.micaelli@cea.fr

Abstract—**The present paper discusses an experimental procedure for designing a suitable coating for Microelectromechanical systems (MEMs) based 3-axis force sensors. Several coating shapes, sizes and materials were tested. The coated sensors were calibrated and tested in order to characterize the effect of the coating on the sensor characteristics such as measurement dynamic range and resolution, the linearity of the response, as well as the impulse response of the system. Finally guidelines for optimal coating of the sensor are proposed.**

Keywords–force; sensor; MEMs; protection; coating

I. INTRODUCTION

The development of Microelectromechanical systems (MEMs) sensors was a revolution that produced small and cheap sensors. This technology allowed massive production of inexpensive and small sensors.

In tactile sensing field, force/torque MEMs based sensors such as presented in [1], [2] and [3] have allowed low cost and highly integrated touch sensing. This type of sensors has shown good characteristics such as linear behavior, low hysteresis, and good accuracy. However, because of their size and fragility, these systems suffer from two major problems:

- The sensitive area of these sensors is small
- The maximal forces and torques that this kind of system could support is low.

For example, the sensor presented in [1] has a maximum force of 1 N and the sensor presented in [3] has a maximum force of 2 N. For most tactile applications, such as object manipulation, in robotics manipulation tasks the range of forces that the sensor should support must be at least 10 N [4].

To solve the problem of measurement range, one solution consists in making bigger silicon based sensors, with bigger supports. However, due to technology considerations, the size of the sensor can not be big enough to cover a large surface which doesn't solve the small sensitive area problem. In addition, using more silicon would significantly increase the sensor cost. Another possible solution consists in protecting the sensor with an elastic coating layer, as shown in [5] or [6]. This solution distributes the forces between the sensitive part of the sensor and the area around which increases the sensor dynamic range. This solution provides protection to the sensor, increases the sensitive surface area and enables the sensor to be interfaced with an external frame for intrinsic tactile sensing such as presented in a previous work [7].

Coating the sensor can have many drawbacks such as the introduction of non linearity and hysteresis. Depending on the used elastic material, a relaxation phenomenon may appear and significantly change the sensor response to external force. The coating increases the dynamic measurement range by distributing the force between the sensor and the surface around which reduces the sensor resolution. Finally, the analysis of the forces applied on any point of the surface is complex. In [6], the authors use a spherical coating geometry to create a soft fingertip. The system could estimate the forces applied during the contact with an external object as well as detect the early slippage. In [5], the authors made a specific geometry to ensure that the contact is established on the top flat surface of the coating. Both papers use polyurethane as protection material.

In all review work about the protection of MEMs force sensors as [5], [6], [8], [9] or [10] they do not analysed more than one coating, and do not discuss why the specific coating shape, size and material has been selected. The goal of this paper is to provide guidelines for the design and construction of the coating for MEMs force sensors supported with experimental results and comparison between various predefined coatings. The objective is to identify the coating shape, size and material that provides the lowest alteration to the sensor characteristics while increasing its dynamic range and providing protection against high forces.

This paper is organized as follow: Section 2 presents the 3-axis MEMs force sensor used in our experiments as well as its initial characteristics. Section 3 presents different coatings used to protect the sensor and as well as their design and construction process. In Section 4, the characterization of each protected sensor is presented. In Section 5, the resistance to high applied forces has been tested for two of the coated sensors. Finally, optimal coating guidelines are deduced.

II. 3-AXIS FORCE MEMS SENSOR

The force sensor operates on the principle presented in [5]. This consists of eight strain sensitive elements that are attached to a stem. All these elements are made of the same silicon crystal and have a geometry shown in Figure 1.

In this case, the sensor is made of a monocrystalline silicon element, where the sensitive elements are eight piezoresistors, i.e., the resistance value varies according to their deformation. They are made by doping the underside of the silicon membrane. The piezoresistors are divided according to the x and y

Copyright (c) IARIA, 2016. ISBN: 978-1-61208-494-7

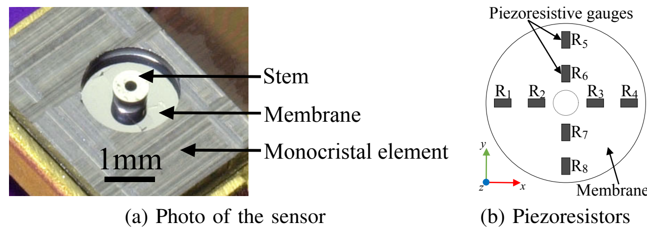

(a) Photo of the sensor (b) Piezoresistors

Figure 1. Sensor structure

axes defining the plane tangential to the membrane as shown in Figure 1b. The eight piezoresistive elements have a similar resistance value R_i at rest, and are placed so that they are constrained symmetrically upon application of a force along an axis x, y or z. Figure 2 shows schematically the deformation of the membrane during the application of a normal force F_z or tangential forces F_x, F_y in the plane of the membrane.

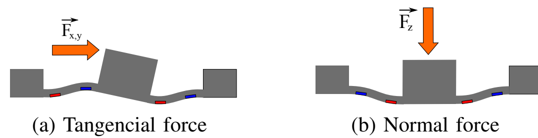

(a) Tangencial force (b) Normal force

Figure 2. Transversal view of the sensor

The piezoresistors are associated to each other in a Wheatstone bridge arrangement according to x and y axis, as shown in Figure 3.

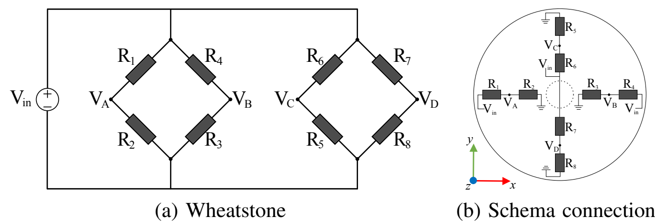

(a) Wheatstone (b) Schema connection

Figure 3. Configuration and distribution of the piezoresistors

Once a force is applied to the stem, the membrane is warped. This causes the compression or the stretching of the piezoresistors along x and y axis, leading to a change in their resistance values. The resistance variation affects the potentials $V_{A,B,C,D}$. The three voltages u_x, u_y and u_z proportional to the applied forces can be calculated as follows:

$$\vec{u} = \begin{bmatrix} u_x \\ u_y \\ u_z \end{bmatrix} = \begin{bmatrix} -a_1 & a_1 & 0 & 0 \\ 0 & 0 & a_2 & -a_2 \\ a_3 & a_3 & -a_3 & -a_3 \end{bmatrix} \begin{bmatrix} V_A \\ V_B \\ V_C \\ V_D \end{bmatrix} \quad (1)$$

where a_1, a_2 and a_3 are identified measurements gains. As presented in [5], in theory, the measurements of the forces are independent. In practice, there is a cross-talk between the axes of the sensor. The forces are estimated as follows:

$$\vec{f} = \begin{bmatrix} f_x \\ f_y \\ f_z \end{bmatrix} = \begin{bmatrix} S_{xx} & S_{xy} & S_{xz} \\ S_{yx} & S_{yy} & S_{yz} \\ S_{zx} & S_{zy} & S_{zz} \end{bmatrix} \begin{bmatrix} u_x \\ u_y \\ u_z \end{bmatrix} - \begin{bmatrix} b_x \\ b_y \\ b_z \end{bmatrix} \quad (2)$$

where S_{ij} are the components of the sensitivity matrix, $u_{x,y,z}$ is the vector of measured voltages, and $b_{x,y,z}$ are the components of the bias vector which is the voltages measured when no forces are applied.

A. Characteristics of the sensor

The sensor has a linear behavior with respect to normal and tangential forces because of the mono-crystalline nature of the sensor and the elasticity of silicon. The used sensor has the following characteristics:

- Membrane radius: $1000\,\mu\text{m}$
- Membrane thickness: $100\,\mu\text{m}$
- Stem radius: $575\,\mu\text{m}$
- $S^{-1}_{xx,yy}$ Sensitivity : $(42.5 \pm 1.5)\,\text{mV/N}$
- S^{-1}_{zz} Sensitivity: $(150.00 \pm 0.25)\,\text{mV/N}$
- F_z max pressure. before deteriorating: $1.5\,\text{N}$
- $F_{x,y}$ max strength. before deteriorating: $1\,\text{N}$
- $\max \Delta U_{x,y}$ maximum voltage variation before the deteriorating in tangential forces: $42.5\,\text{mV}$
- $\max \Delta U_z$ maximum voltage variation before the deteriorating in normal forces: $225\,\text{mV}$
- The sensor is $5\,\text{mm}$ long, $3.5\,\text{mm}$ wide, and $0.8\,\text{mm}$ high regardless of the stem.
- Cut-off frequency: $54\,\text{Hz}$ to $60\,\text{Hz}$

All sensitivity values are given for a supply voltage of $5\,\text{V}$.

III. Considered Sensor Coating

In order to protect the sensor and increase its sensitivity range, the sensor was protected as shown in [5]. The protection is made by deposing an elastic material over the sensor so that the forces exerted on the material will be distributed between the sensor and the support.

The chosen elastic material is polyurethane. This choice is entirely based on previous work results in determining the proper type of protection, [5] or [6]. The MEMs sensor is integrated and connected to a round PCB as shown in Figure 4 and several protections were implemented and tested.

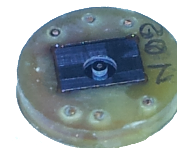

Figure 4. MEMs force sensor connected and mounted in PCB

In this document, 5 protections are dealt with as shown in Figure 5.

These sensors were chosen to be tested in order to determine the following points:

Copyright (c) IARIA, 2016. ISBN: 978-1-61208-494-7

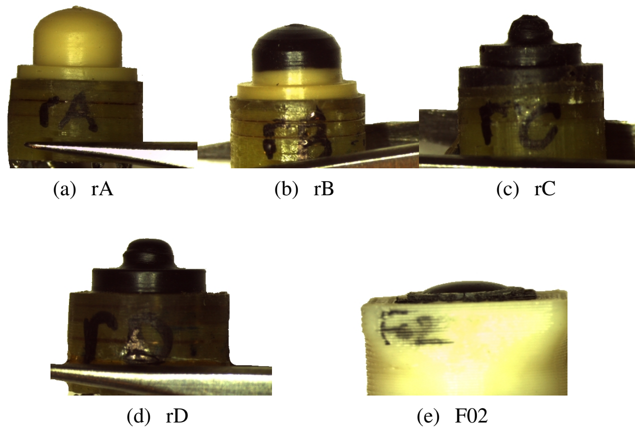

(a) rA (b) rB (c) rC

(d) rD (e) F02

Figure 5. Coated MEMs force sensors

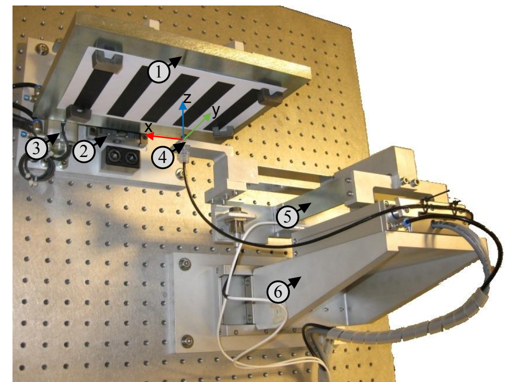

1.Rigid surface	4.Force sensor
2.Precision screw	5. Reference force sensor
3.Pneumatic actuator	6. Linear actuators

Figure 6. Testing system

The optimal construction material: The sensors are protected with two different polyurethane resins. The difference between the two tested materials is essentially in the hardness:

- the black polyurethane has a hardness of Shore 80
- the beige polyurethane has a hardness of Shore 40

The sensors rC, rD and F02 are protected with black polyurethane, rA with beige polyurethane, and the sensor rB is composed of half of each.

The influence of height: Sensors rC and rD have the same shape, the same material but different height in order to establish a relationship between the coating height and the response of the sensor.

The influence of shape: Differences in behavior between the forms of protection.

The coating procedure: Sensors rA, rB, rC and rD are made from a mold, and the protection F02 by pouring the material above the sensor.

IV. Coated Sensor Characterization

In this section, a relatively low force range is used in order to determine the sensor characteristics without pushing it to its maximum supported force.

A. Experimental test bench

In order to calibrate and qualify the different coatings, a testing system (Figure 6) was created. This system uses a reference force sensor developed in [5] mounted on two linear actuators (Lx80F40 Linax Jenny Science) placed along the x and y axes. A precision screw and a pneumatic actuator are used to move a rigid plate parallel to the reference force system. The data acquisition system is a national instruments acquisition board (DAQ) PXI-6225 at a frequency of $1\,\mathrm{kHz}$.

B. Characterization methodology

The following measurement methodology is performed:

- Fix the sensor to measure, in its support, in the end effector.
- Without applying any force, begin to acquire the voltages $\vec{u}$ in order to calculate the offset $\vec{b}$
- The sensor and the rigid surface are brought into contact by the precision screw, until a force of $(1.3 \pm 0.2)\,\mathrm{N}$ is exerted, and is varied manually without exceeding $1.6\,\mathrm{N}$ force.
- The two linear motors move along a predefined path, to exert tangential forces on the sensor
- When the motion terminates, the contact is automatically removed by a pneumatic actuator
- The acquisition system is stopped

The defined trajectory is designed so that the force exerted on the sensor sweeps through all of the measurable force range, i.e., explore both the positive and negative forces in the x and y axes without breaking the sensor. Unfortunately, the contact between the 3-axis force sensor and the rigid surface has a small friction coefficient, that does not allow exertion of tangential forces through all of the measurable force range. The trajectory is shown in Figure 7. The used trajectory is square in order to minimize the effects of cross-talking between the axes.

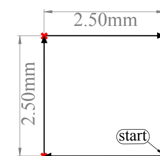

Figure 7. Trajectory for the sensor characterization

The first portion of the acquired signal is used to remove the sensor offset. At the beginning, the exerted force is null, thus the measured voltages vector $\vec{u}$ is equal to the bias vector $\vec{b}$.

$$\vec{f} = 0 \Rightarrow \vec{u} = \vec{b} \tag{3}$$

The sensitivity matrix of each sensor can be estimated using least squares method as follows :

$$\{l_i, \mathbf{S}_i\} = \underset{l_i, \mathbf{S}_i}{\operatorname{argmin}} \sum_{j=1}^{n} \left(\vec{\mathrm{ref}}_j - \vec{f}_j \right)^2 \tag{4}$$

Copyright (c) IARIA, 2016. ISBN: 978-1-61208-494-7

where $\vec{\text{ref}}_j$ is the reference measurement of forces at sampling time j, and $\vec{f_j}$ is the forces calculated by equation 2 at sampling time j. n is the number of samples.

C. Characterization results

At least two measures of each of the five mentioned sensors were made. Half of the taken measures is used to calculate the sensitivity matrix and the other is used to validate the calibration.

The results of the experiments are shown in the Figure 8. The first row of the Figure 8 presents the results for the measurement set used to calibrate the sensor. The second row of Figure 8 presents the results for the measurement set used to validate the calibration. Figure 8 shows the acquired data at the point where the contact was removed. In fact, when the contact is released using the pneumatic actuator, the reference sensor begins to vibrate because the deformation due to the introduced forces creates a mass-sting system, consequently the last part of the acquired data of the measures is not used to calibrate the sensor since the reference is not accurate.

Table I presents the error statistics between the reference system and each of the 3 axis force sensors.

	Measure	Mean error	Max error	Standard deviation
rA	f_x	$-3.36\,\text{mN}$	$46.31\,\text{mN}$	$11.82\,\text{mN}$
	f_y	$-8.44\,\text{mN}$	$65.00\,\text{mN}$	$15.67\,\text{mN}$
	f_z	$13.89\,\text{mN}$	$52.78\,\text{mN}$	$11.98\,\text{mN}$
rB	f_x	$-2.09\,\text{mN}$	$64.19\,\text{mN}$	$12.78\,\text{mN}$
	f_y	$9.29\,\text{mN}$	$70.34\,\text{mN}$	$16.56\,\text{mN}$
	f_z	$3.90\,\text{mN}$	$33.42\,\text{mN}$	$7.79\,\text{mN}$
rC	f_x	$-19.85\,\text{mN}$	$133.14\,\text{mN}$	$40.70\,\text{mN}$
	f_y	$-24.37\,\text{mN}$	$144.11\,\text{mN}$	$35.92\,\text{mN}$
	f_z	$5.82\,\text{mN}$	$37.65\,\text{mN}$	$8.19\,\text{mN}$
rD	f_x	$-3.77\,\text{mN}$	$54.34\,\text{mN}$	$18.17\,\text{mN}$
	f_y	$-2.87\,\text{mN}$	$51.63\,\text{mN}$	$11.92\,\text{mN}$
	f_z	$-1.52\,\text{mN}$	$31.25\,\text{mN}$	$11.56\,\text{mN}$
F02	f_x	$72.81\,\text{mN}$	$190.33\,\text{mN}$	$63.86\,\text{mN}$
	f_y	$-10.53\,\text{mN}$	$69.15\,\text{mN}$	$16.67\,\text{mN}$
	f_z	$28.94\,\text{mN}$	$135.17\,\text{mN}$	$40.19\,\text{mN}$

Table I. Error statistics coated sensor

The graphics of the relation between the reference forces against the calculated forces are shown in the third row of Figure 8.

To characterize the dynamic behavior of the sensor in the z axis, the reference data at the instant when the contact is released is replaced by a step function in the system input (in order to avoid the reference sensor vibration problem). Using these signals, the transfer function for each coated sensor is calculated. Taking as reference the following two characteristic transfer functions:

- Second order over-damped system

$$\frac{f_z(s)}{f_{z\text{real}}(s)} = \frac{K_p}{(1+\text{Tp}_1 s)(1+\text{Tp}_2 s)} \tag{5}$$

- System with two poles and one zero

$$\frac{f_z(s)}{f_{z\text{real}}(s)} = \frac{a_1 s + a_2}{s^2 + a_3 s + a_4} \tag{6}$$

The constant values K_p, Tp_1, Tp_2, or $a_{1,2,3,4}$ are found for each sensor. These values can be calculated in different ways. For example by the method of Harriot for over-damped second order systems or by minimizing the error between the input and output. The System Identification toolbox of MATLAB was used in order to easily determine these values. As it can be deduced from the fourth row in Figure 8, sensors rA and rB have a transfer function that fits with a second order transfer function 5. The other three sensors have a well pronounced relaxation phenomenon. As a consequence, their transfer function fits better with the one of a system with two poles and one zero presented in equation 6. The transfer functions calculated for sensors are shown in the Figure.

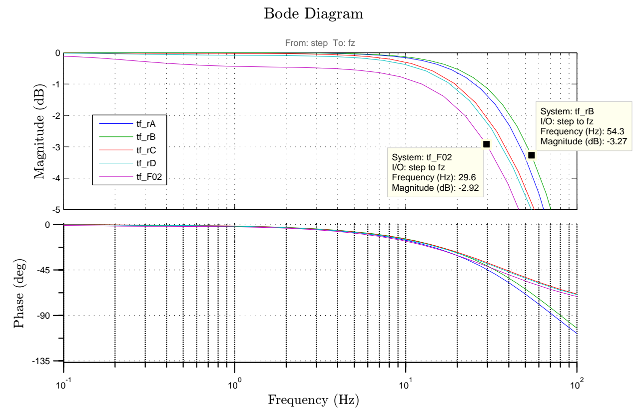

Figure 9. Frequency response and phase of the coated force sensors

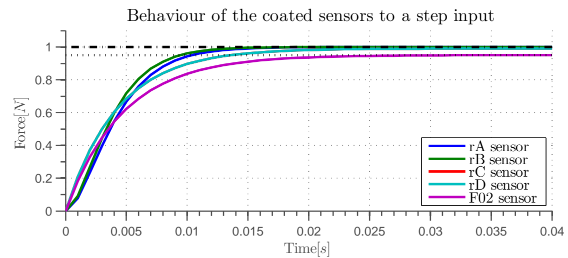

Figure 10. Behavior of the coated force sensors to a step input

	S_{xx}^{-1}	S_{yy}^{-1}	S_{zz}^{-1}	Cut-off freq
rA	$0.675\,\text{mV/N}$	$0.675\,\text{mV/N}$	$9.5\,\text{mV/N}$	$\approx 45\,\text{Hz}$
rB	$0.425\,\text{mV/N}$	$0.370\,\text{mV/N}$	$10.5\,\text{mV/N}$	$\approx 50\,\text{Hz}$
rC	$0.8\,\text{mV/N}$	$0.8\,\text{mV/N}$	$15\,\text{mV/N}$	$\approx 35\,\text{Hz}$
rD	$0.63\,\text{mV/N}$	$0.63\,\text{mV/N}$	$13\,\text{mV/N}$	$\approx 34\,\text{Hz}$
F02	$0.74\,\text{mV/N}$	$0.4\,\text{mV/N}$	$10.5\,\text{mV/N}$	$\approx 30\,\text{Hz}$

Table II. Error statistics coated sensor

Bode plot and phase, calculated from systems presented in Figure 8, are shown in Figure 9.

The modelled cutoff-frequency of the sensors varies between $\approx 30\,\text{Hz}$ for the F02 and $\approx 50\,\text{Hz}$ for the rB. The theoretical performance of the sensors to a step signal is shown in Figure 10.

The characteristics of sensitivity and cut-off frequency of each sensor are presented in Table II.

The results were obtained using a linear model of the behavior of the sensor.

Copyright (c) IARIA, 2016. ISBN: 978-1-61208-494-7

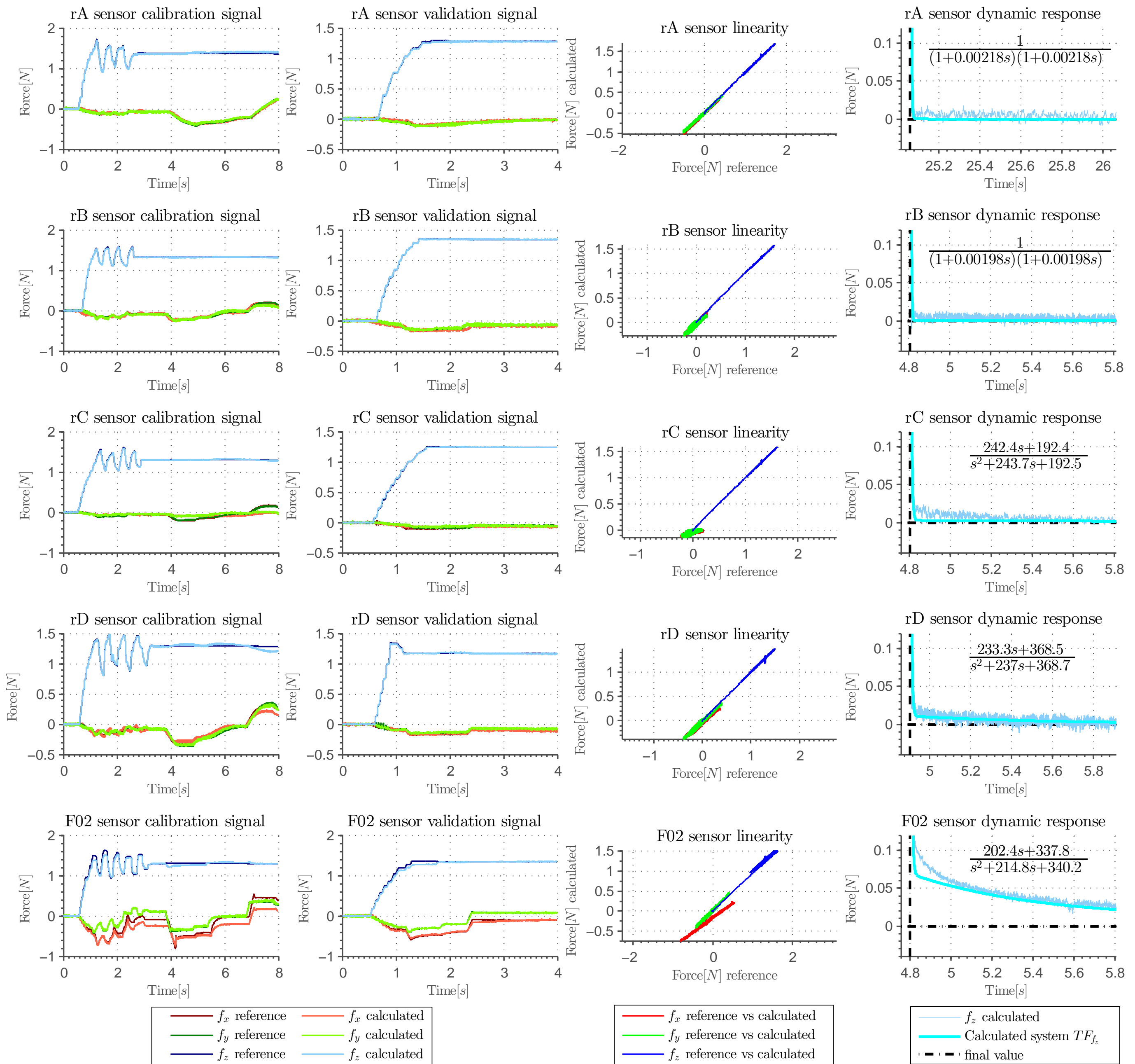

Figure 8. Results of the coated sensor characterization

D. Results Analysis

From Figure 8 and Table I, it is clear that sensors rA, rB and rD have similar behaviors and good matching of the estimated forces with respect to the reference ones. However, sensors rC and F02 have errors that are almost double compared to the others.

Figure 8 shows that sensors rA, rB and rD preserve the linear behavior between measurements. Additionally, the figure shows that the sensors rC, rD and F02 have a a more significant relaxation phenomenon.

Regarding the set-points evoked in section III. The following analyses are made:

Material to be used: For the beige polyurethane with hardness of Shore 40, the relaxation phenomenon isn't considerable as is shown in Figure 8. Sensors coated directly with this material have a better dynamic behavior (rA and rB). When two materials are combined as for the sensor rB, the problem is that the forces are not distributed evenly in all directions (as shown in the linearity analysis figures).

Influence of height: Sensors rC and rD have the same shape and the same material. However they have very different

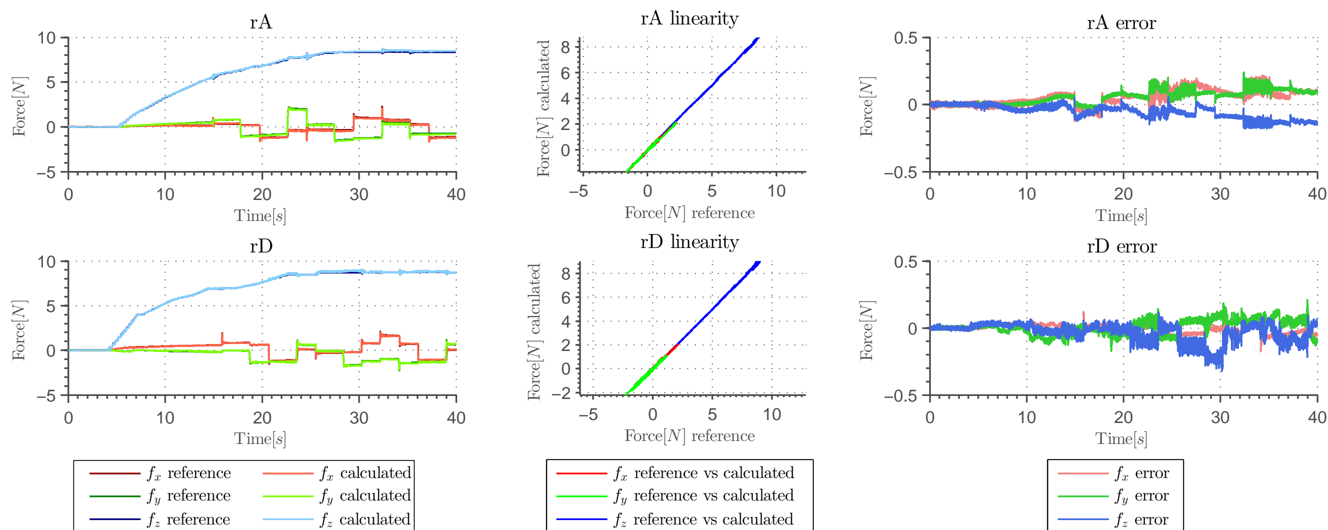

Figure 11. Results of the selected coated sensors

behaviours. The bigger coating height in sensor rC reduces its sensitivity to tangential forces.

Influence of the shape: Three different basic shapes were tested. The coating used in rA and rD has the same best linearity. Those shapes gave the best results. The shapes of sensors F02 and rC have a wide base. This significantly decreases their sensitivity in the shear axes. One of the biggest problems of the coating shape used for the F02 is that the point where the forces are applied is not centered with the sensor.

Manufacturing type of protection: The point of application of forces in the sensor must be well defined, the F02 sensor does not have this characteristic. In fact during the hardening process of the polyurethane, any disturbance in the angle affects the central point position.

V. Resistance to high forces test

The coated sensors that present the best characteristics (rA and rD) are selected for the high force test. The test consists of repeating the same experiment presented in the previous section by applying a higher force range. The test bench system does not allow more than 9 N. In this test, at least 8 N was applied to the sensor. The goal of this test is to verify if the coating preserves its characteristics for the range needed for object manipulation (about 10 N). The results are shown in Figure 11.

As shown in the figure, the sensors preserve their characteristics such as the linearity for the whole range of tested forces. The two systems resisted about 9 N without breaking. Clearly, they could go beyond this range without any problems. After the experiment, no hysteresis was noticed nor was there a change in their sensitivity. A more robust test bench tool could be used to determine the maximum supported force.

VI. Conclusion

This paper presents an experimental procedure for designing a suitable coating for MEMS based 3-axis force sensors. Five different coatings with different shapes, sizes and materials were calibrated, tested and characterized in order to show the effect of the coating. The analysed characteristics were the statistics of error in time, the linearity of the response as well as the impulse response of the system and the final sensitivity of the sensor.

The two sensors with the best characteristics are tested in a larger range showing that this type of coating is desirable to use in protecting MEMs force sensors.

The guidelines proposed in section III for the design and construction of the coating for MEMs force sensors supported with experimental results of section IV were analyzed and the conclusions are:

Coating material: The relaxation of the material should be the fastest possible one. Polyurethane Shore 40 meets this criterion and is advised to be used as a coating material.

Influence of height: A higher coating leads to lower sensor sensitivity to tangent forces. Thus, reducing the coating height is advised.

Influence of the shape: The point where the forces are exerted must be centered, so the tip of the protection must be pointy, and the base should not be too wide.

Manufacturing type of protection: The sensors must be made by molding.

The proposed guidelines can be used to create new coatings, with different range of forces and sensitivities. Consequently the force MEMs sensors can be applied in a larger set of applications.

Further work will focus on the creation of a new coating for a 3-axis force sensor matrix. This matrix can be used for the development of a tactile sensing system for robotics dexterous manipulation.

References

[1] F. De Boissieu, C. Godin, B. Guilhamat, D. David, C. Serviere, and D. Baudois, “Tactile texture recognition with a 3-axial force mems

integrated artificial finger." in *Robotics: Science and Systems*. Seattle, WA, 2009, pp. 49–56.

[2] D. V. Dao, T. Toriyama, J. Wells, and S. Sugiyama, "Micro force-moment sensor with six-degree of freedom," in *Proceedings of 2001 International Symposium on Micromechatronics and Human Science, 2001. MHS 2001*, 2001, pp. 93–98.

[3] K. Kim, K. R. Lee, Y. K. Kim, D. S. Lee, N. K. Cho, W. H. Kim, K. B. Park, H. D. Park, Y. K. Park, J. H. Kim, and J. J. Pak, "3-Axes Flexible Tactile Sensor Fabricated by Si Micromachining and Packaging Technology," in *19th IEEE International Conference on Micro Electro Mechanical Systems, 2006. MEMS 2006 Istanbul*, 2006, pp. 678–681.

[4] H. Yousef, M. Boukallel, and K. Althoefer, "Tactile sensing for dexterous in-hand manipulation in roboticsA review," *Sensors and Actuators A: Physical*, vol. 167, no. 2, pp. 171–187, Jun. 2011. [Online]. Available: http://linkinghub.elsevier.com/retrieve/pii/S0924424711001105

[5] F. d. Boissieu, C. Godin, L. Olmos, B. Guilhamat, D. D. C. Serviere, and D. Baudois, "Artificial touch system based on a MEMS sensor: design, characterization and application to fine texture recognition," *submitted to IEEE Trans. on Robotics*, 2011.

[6] V. A. Ho, D. V. Dao, S. Sugiyama, and S. Hirai, "Development and Analysis of a Sliding Tactile Soft Fingertip Embedded With a Microforce/Moment Sensor," *IEEE Transactions on Robotics*, vol. 27, no. 3, pp. 411–424, Jun. 2011.

[7] A. Ospina, S. Aloui, C. Godin, M. Grossard, and A. Micaelli, "Tactile sensing system for robotics dexterous manipulation based on a matrix of 3-axes force sensors," in *2015 IEEE/RSJ International Conference on Intelligent Robots and Systems (IROS)*, Sep. 2015, pp. 2105–2110.

[8] B. Gray and R. Fearing, "A surface micromachined microtactile sensor array," in *, 1996 IEEE International Conference on Robotics and Automation, 1996. Proceedings*, vol. 1, Apr. 1996, pp. 1–6 vol.1.

[9] L. Beccai, S. Roccella, L. Ascari, P. Valdastri, A. Sieber, M. Carrozza, and P. Dario, "Development and Experimental Analysis of a Soft Compliant Tactile Microsensor for Anthropomorphic Artificial Hand," *Mechatronics, IEEE/ASME Transactions on*, vol. 13, no. 2, pp. 158 –168, Apr. 2008.

[10] R. Candelier, A. Prevost, and G. Debrgeas, "The Role of Exploratory Conditions in Bio-Inspired Tactile Sensing of Single Topogical Features," *Sensors (Basel, Switzerland)*, vol. 11, no. 8, pp. 7934–7953, Aug. 2011. [Online]. Available: http://www.ncbi.nlm.nih.gov/pmc/articles/PMC3231713/